

THE PENNSYLVANIA STATE UNIVERSITY
SCHREYER HONORS COLLEGE

DEPARTMENT OF METEOROLOGY AND ATMOSPHERIC SCIENCE

Air-Sea Analysis of Marine Heatwaves in the Northeastern Pacific

CATHERINE KOHLMAN
SPRING 2022

A thesis
submitted in partial fulfillment
of the requirements
for a baccalaureate degree
in Meteorology and Atmospheric Science
with honors in Meteorology and Atmospheric Science

Reviewed and approved* by the following:

Sukyoung Lee
Professor of Meteorology
Thesis Supervisor

Raymond Najjar
Professor of Oceanography
Honors Adviser

* Electronic approvals are on file.

ABSTRACT

A marine heatwave is a region of large temperature anomalies in the uppermost part of the ocean. Recently these events have caught the attention of many scientists due to their increasing intensity, frequency, and persistence with climate change and the increased impacts on the chemistry and biology of the ocean. The northeastern Pacific experienced two strong marine heatwaves (2013-2015 & 2019) that caused havoc on fisheries, driving the necessity to understand how these events are created and how we can predict their impacts. Currently, there is a great knowledge gap in how marine heatwaves in the northeastern Pacific form and how the role of the ocean and atmosphere may influence their development. The study presented here performs a comprehensive look at 15 positive summertime temperature anomaly events in the northeastern Pacific from 1979 to 2020 using ERA5 and JRA-55 reanalysis datasets. The surface energy budget analysis performed suggests that the summertime sea surface temperature anomalies are heavily influenced by a change in the atmospheric circulation above the northeastern Pacific Ocean allowing anomalous downward solar radiation to drive the warming. This change in circulation is shown, through model simulations, to be connected to anomalous latent heating in the central tropical Pacific and the Maritime Continent that initiate Rossby wave propagation from the tropics to the northeastern Pacific. The results of this study offer a comprehensive view of multiple summertime events that can be used to increase the predictability of future summertime marine heatwaves. Increasing the predictability of marine heatwaves will improve our understanding and ability to manage the associated impacts of these anomalous events.

TABLE OF CONTENTS

LIST OF FIGURES	iii
LIST OF TABLES	iv
ACKNOWLEDGEMENTS	v
Introduction.....	1
Focus Region	4
Reanalysis Data.....	5
<i>ERA5</i>	5
<i>JRA-55</i>	5
<i>ONI Index</i>	6
Methodology	7
<i>Warm event definition</i>	7
<i>Surface Energy Budget</i>	7
<i>Model Simulation</i>	8
Results.....	10
<i>Northeastern Pacific Sea Surface Temperature Anomalies</i>	10
<i>Surface Energy Budget Analysis</i>	15
<i>Summertime External Forcing</i>	19
Discussion	30
Conclusion	33

LIST OF FIGURES

- Figure 1. Blank map illustrating the NEP study region used in the study. The black box represents the region of interest: 43-53°N, 215-228°E..... 4
- Figure 2. Timeseries of detrended monthly sea surface temperatures (°C) in the NEP focus region (1979-2020). 10
- Figure 3. Seasonally averaged detrended sea surface temperature anomalies (°C) in the NEP focus region (1979-2020). 11
- Figure 4. Timeseries of detrended Jun-Aug sea surface temperatures (°C) in the NEP focus region (1979-2020) with warm events identified by open red circles. The three filled red circles represent three warm events that occurred during an El Niño event that occurred in Jun-Aug. 12
- Figure 5. Observed sea surface temperature composite anomalies (°C) in the NEP (a) in Mar-May, prior to Jun-Aug warm events and (b) during warm events in Jun-Aug. 14
- Figure 6. Surface energy budget component composite anomalous (a & b) R-G, (c & d) downward net solar radiation, (e & f) downward net longwave radiation, (g & h) downward sensible heat flux, and (i & j) downward surface latent heat flux contributions to the SSTAs for Mar-May (left column) and Jun-Aug (right column) in K per decade (Equation 2). 16
- Figure 7. Observed 300 mb eddy streamfunction composite anomalies ($m^2 s^{-1}$) during warm events in Jun-Aug. 19
- Figure 8. Composite anomalies for cloud coverage (negative = less clouds & positive = more clouds) in Jun-Aug for warm events..... 20
- Figure 9. Observed latent heat anomalies ($kg m^{-3}$) averaged throughout the atmospheric column during warm events in Jun-Aug. Dashed boxes represent regions of interest for anomalous tropical heat forcing. 21
- Figure 10. Model output of Jun-Aug 300 mb eddy streamfunction anomalies ($m^2 s^{-1}$) forced by the global heating field shown in Figure 9. 22
- Figure 11. Pattern correlation map of 30°x30° patches (ranging from -30°-60°N to 30°-270°E) of model outputs of given patch observed Jun-Aug latent heating anomalies (represented by contoured diamond in the center of a given patch) correlated to observed of Jun-Aug 300 mb eddy streamfunction anomalies ($m^2 s^{-1}$) (a) globally and (b) within a 30°-70°N and 170°-250°E region (black). 24
- Figure 12. JJA model output 300 mb eddy streamfunction anomalies ($m^2 s^{-1}$) from the patch, 0°-30°N and 90°-120°E, that had the highest correlation coefficient (0.76 as

shown in Table 2) when correlated to the atmospheric circulation within 30°-70°N and 170°-250°E. 27

Figure 13. JJA model output 300 mb eddy streamfunction anomalies ($\text{m}^2 \text{s}^{-1}$) from (a) the central tropical Pacific, (b) the Maritime Continent, and (c) both the central tropical Pacific and Maritime Continent combined. Dashed boxes representing regions of interest for heat forcing. * 28

LIST OF TABLES

Table 1. Warm events with associated sea surface temperature values (°C; in descending order) and ONI index recorded during Jun-Aug.....	13
Table 2. Locations of the top positively correlated patches for JJA 300 mb streamfunction anomalies.	26

ACKNOWLEDGEMENTS

I would like to thank my thesis supervisor, Sukyoung Lee, for encouraging me to pursue my research interests while pushing me to learn how to run the GFDL model and interpret the results.

I would also like to thank Tom Murphree who has been my mentor for multiple years. He has always given me the confidence and excitement to look for new research questions and has always encouraged me to pursue my passions.

The work in this thesis could not have been completed without the patient assistance from Allen Mewhinney, Ph.D. student, and Dong Won Kim, Ph.D. candidate. No matter how many questions and/or issues with learning how to force the atmospheric model, they always welcomed me with an open door.

I would also like to thank Steven Feldstein, Cory Baggett, Fan Wu, Changyun Yoo, and Mingyu Park for listening to my results and providing fantastic feedback to help push the work in new ways in weekly group meetings.

I would also like to thank Raymond Najjar for being my honors advisor, supporting my research endeavors throughout my undergraduate career, teaching me so many oceanographic concepts, and for the feedback for this thesis.

This work would not have been accomplishable without the constant support from my friends and family who made my undergraduate experience the most enriching four years of my life thus far.

Introduction

As the climate constantly changes (naturally and anthropogenically), changes are often seen day-to-day in the atmosphere and oceans around us. In the past decade, marine heatwaves (MHWs) have caught the attention of the oceanographic community due to their intensity, duration, and socioeconomic and ecosystem impacts.

Simply defined, a MHW is a region in the upper ocean that is anomalously warm for a discrete time. More quantitatively, MHWs have been proposed to be defined as sea surface temperatures (SSTs) exceeding the varying 90th percentile of the locally observed 30-year climatology (Hobday et al. 2016). Other definitions are often used to distinguish different types of MHWs based on intensity and duration (Hobday et al. 2018). MHWs defined above the 99th percentile were found to have doubled in frequency between 1982 and 2016 (Frölicher et al. 2018), suggesting that these events are influenced by climate change. Laufkötter et al. (2020) suggest that one extreme MHW, ‘The Blob’ in the northeastern Pacific (NEP) occurring from 2013 to 2015, would not have been possible without anthropogenic global warming. These events have been observed around the world (Holbrook et al., 2019) and can have different, yet dramatic, impacts on marine ecosystems, biodiversity, and fishery economics (Cheung and Frölicher 2020 and Smale et al. 2019).

MHWs occur globally and are expected to be more intense and persistent as the climate continues to be changed (Tanka and Van Houtan, 2022; Holbrook et al., 2019; Frölicher et al.

2018). MHWs around the globe that have been studied in depth include, but are not limited to, the Mediterranean Sea in 2003 (Sparnocchia et al. 2003), off the Australian coast in 2011 and 2015-2016 (Pearce and Feng 2013; Oliver et al. 2017; Benthuyesen et al. 2018), the South Atlantic in 2013-2014 (Rodrigues et al. 2019), and the NEP in 2013-2015 and 2019 (Bond et al. 2015; Amaya et al. 2020). Although the rising global SSTs are the dominant driver in many MHW events (Frölicher et al. 2018), the causes of MHWs are also from a variety of both local and remote physical processes – both atmospheric and oceanic (Holbrook et al. 2019). These processes include but are not limited to, air-sea heat exchange, oceanic advection, and increased stratification in the upper ocean (Oliver et al. 2021; Amaya et al. 2020; Bond et al. 2015). Different climate modes, such as the El Niño Southern Oscillation (ENSO), may also increase the probability of a MHW occurring (Holbrook et al. 2019).

The NEP has been an area of interest regarding MHWs with two major MHW events occurring in the past decade. In the winter of 2013, a ‘Blob’ of sea surface temperature anomalies (SSTAs) occurred and persisted well into 2015 (Bond et al. 2015), forcing many fisheries on the Pacific Coast to close due to associated toxic algae blooms and whale entanglements (Cheung and Frölicher, 2020; Holbrook et al. 2019). A few years later, a similar, yet stronger, SSTA ‘Blob’ appeared in the spring of 2019 that persisted until the fall of 2019 (Amaya et al. 2020) and is often referred to as the Blob 2.0. The impacts of the 2019 MHW are still not well known.

To date, the major atmospheric and oceanic drivers of each of these events are still not well understood. The 2013-2015 MHW has been suggested to be a result of atmospheric

anomalies (i.e., weaker-than-normal surface winds) with teleconnections to the tropics (Joh and Di Lorenzo 2017; Di Lorenzo et al. 2016). Fewings and Brown (2019) suggested that the net air-sea heat flux anomaly was small, but the shoaling mixed layer depth (MLD) played a major role in the life cycle of the 2013-2015 MHW. Amaya et al. (2021) suggested that the main driver of the 2019 MHW was the record shallow summer MLD trapping solar heat in the upper ocean that was influenced by a change in the upper atmospheric circulation directly above the NEP. There is also an ongoing debate about the possible connection to ENSO (Bond et al. 2015; Holbrook et al. 2019). From the studies that have been performed for the NEP MHWs, the atmospheric and oceanic connections to the drivers, life cycle, and conclusion of such events are not understood in a way to tell a clean story and what a future MHW and associated impacts event might entail.

Unlike most prior studies, we investigate multiple (i.e., not a single case study) MHW-like events in the NEP during the summertime. We provide insight into the tropical latent heat external forcing and formation of past MHWs that can aid in the prediction of future MHWs by focusing on two main research questions:

1. Is the atmosphere-ocean energy exchange in the NEP important in generating NEP MHWs?
2. Is there any evidence of tropical latent heat forcing aiding the energy exchange and development of NEP MHWs?

Focus Region

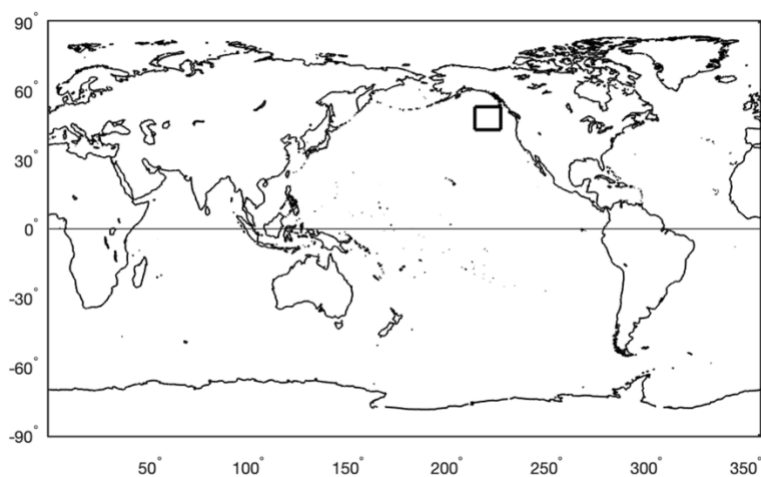


Figure 1. Blank map illustrating the NEP study region used in the study. The black box represents the region of interest: 43-53°N, 215-228°E

Motivated by previous studies and the increasing need to understand and predict the ocean extremes in the Pacific Northwest, the region of focus of the 15 events used in this study is defined by the region of NEP within 43-53°N, 215-228°E (Figure 1). We selected this region as a compromise of the areas used by Amaya et al. (2020) and Bond et al. (2015) as well as our own analyses of SSTAs locations in the NEP during the summers of 1979-2020.

Reanalysis Data

ERA5

In this study, we use monthly averaged sea surface and air temperature, downward net solar radiation, downward net longwave radiation, downward sensible heat flux, downward latent heat flux, cloud coverage, and streamfunction data from the fifth generation of the European Centre for Medium-Range Weather Forecasts (ECMWF) atmospheric reanalysis (ERA5) daily data from 1979 to 2020 (Hersbach et al. 2020). We chose this period because of the large amounts of satellite data that were available during this period for reanalysis. The length of this period also provides a relatively large number of MHW events. For all variables, a $2.5^{\circ} \times 2.5^{\circ}$ horizontal grid spacing is used. Our study focuses on the spring, Mar-May (MAM), and the summer, Jun-Aug (JJA), seasons. Anomalies are computed from the baseline period of 1981-2010.

We removed the zonal mean from the 300 mb streamfunction anomalies to best show the atmospheric circulation changes. These are considered ‘eddy streamfunction anomalies’ from this point forward.

The ERA5 data are available at:

<https://www.ecmwf.int/en/forecasts/datasets/reanalysis-datasets/era5>

JRA-55

The latent heating rate fields are created using monthly averaged daily large-scale condensational heating and convective heating fields from the Japanese 55-year Reanalysis (JRA-55, Kobayashi et al. 2015), focusing on 1979-2020. We combine the large-scale

condensational heating and convective heating fields into one variable to display all latent heating anomalies. All 36 levels and a 2.5°x2.5° horizontal grid spacing are used. Anomalies are computed from the baseline period of 1981-2010.

The JRA-55 data are available at:

<https://climatedataguide.ucar.edu/climate-data/jra-55>

ONI Index

To indicate which events are part of a given ENSO phase, we use the Oceanic Niño Index (ONI). The ONI is a 3-month running mean of Extended Reconstructed Sea Surface Temperature version 5 (ERSST.v5) SST anomalies (based on a 5-year running 30-year base period) within 5°N-5°S, 120°-170°W, or the Niño 3.4 region (NOAA, 2019b). Seasonally averaged ONI index values above 0.5 are considered an El Niño, and seasonally averaged ONI indices below 0.5 are considered a La Niña.

The ONI data are available at:

https://origin.cpc.ncep.noaa.gov/products/analysis_monitoring/ensostuff/ONI_v5.php

Methodology

Warm event definition

This study defines MHWs, or warm events, inspired by the widely accepted technical definition of a MHW: persistent SSTAs that exceed the seasonally varying 90th percentile threshold for more than five consecutive days (Hobday et al. 2016). Hobday et al. (2018) evolved this definition to include different categories to define MHWs based on duration and intensity. We chose to qualify a warm event in this study as a summer SSTA event ranking in the top 15 of the study years (1979-2020) based on area-averaged detrended JJA SST data from 1979-2020 in the NEP (Figure 1). The 15 qualifying years are considered ‘warm events’ and capture the two most recent MHWs along with prior events that were selected based on the occurrence of upper tercile SSTAs in the NEP region for JJA. We use linear regression to determine the 1979-2020 linear trend and removed the trend to analyze the data so that the long-term climate change signal was removed.

Surface Energy Budget

Components of the surface energy budget for warm events are analyzed using the following equation (Equation 1) which is described in more detail in Clark et al. (2021):

$$G - R = SSR + STRD + (-\epsilon\sigma SST^4) + SSHF + SLHF \quad (1)$$

Where G denotes a thin surface layer of energy storage, R is the residual, SSR is the net downward solar radiation, $STRD$ is the net downward longwave radiation, $SSHf$ is the downward sensible heat flux, and $SLHF$ is the downward latent heat flux all in units of $W m^{-2}$.

Similar to Clark et al. (2021), after taking the differential of Equation 1 and letting $STRD = -\varepsilon\sigma T^4$ (where ε is the emissivity - assumed to be approximately 1, σ is the Stefan-Boltzman constant, and T is the 2 m air temperature in units of Kelvin), we arrive at Equation 2 to express the contributions to the change in SST (K/decade):

$$\delta SST = \frac{\delta SSR + \delta STRD + \delta SSHf + \delta SLHF + \delta(R-G)}{4\varepsilon\sigma T^3} \quad (2)$$

The quantity $\delta(R - G)$ represents the residual which includes ocean divergence and temperature advection.

Model Simulation

To identify potential tropical latent heat forcing, we modify the spectral dynamical core model from the NOAA Geophysical Fluid Dynamics Laboratory (GFDL) to represent warm event conditions. The model is run for 20 days with a vertical resolution of 28 sigma levels and at a horizontal resolution of 42 triangular levels. A fourth-order parameterization for Newtonian cooling and Rayleigh friction (Held and Suarez, 1994) are incorporated into the model as well. As in Baggett et al. (2016) and Kim and Lee (2021), a JJA 1979-2020 climatology of zonal and meridional winds, pressure, specific humidity, and temperature is used to create the initial, unbalanced background state. To balance the background state, a forcing term is added after initializing and integrating the model by one time step. This causes the model to evolve only

when a forcing term is added. The forcing, or perturbation, in this experiment is the JRA-55 anomalous large scale and convective heating field anomalies for warm events. Of the 20 days that the model is run, the results for days 10-20 (after the perturbation has been applied) are averaged and displayed in this paper.

Results

Northeastern Pacific Sea Surface Temperature Anomalies

The temporal evolution of NEP SSTs during 1979-2020 (Figure 2) reveals that NEP SSTAs: (a) have increased in magnitude in recent years; (b) show large interannual variation; and (c) tend to be especially strong in summer.

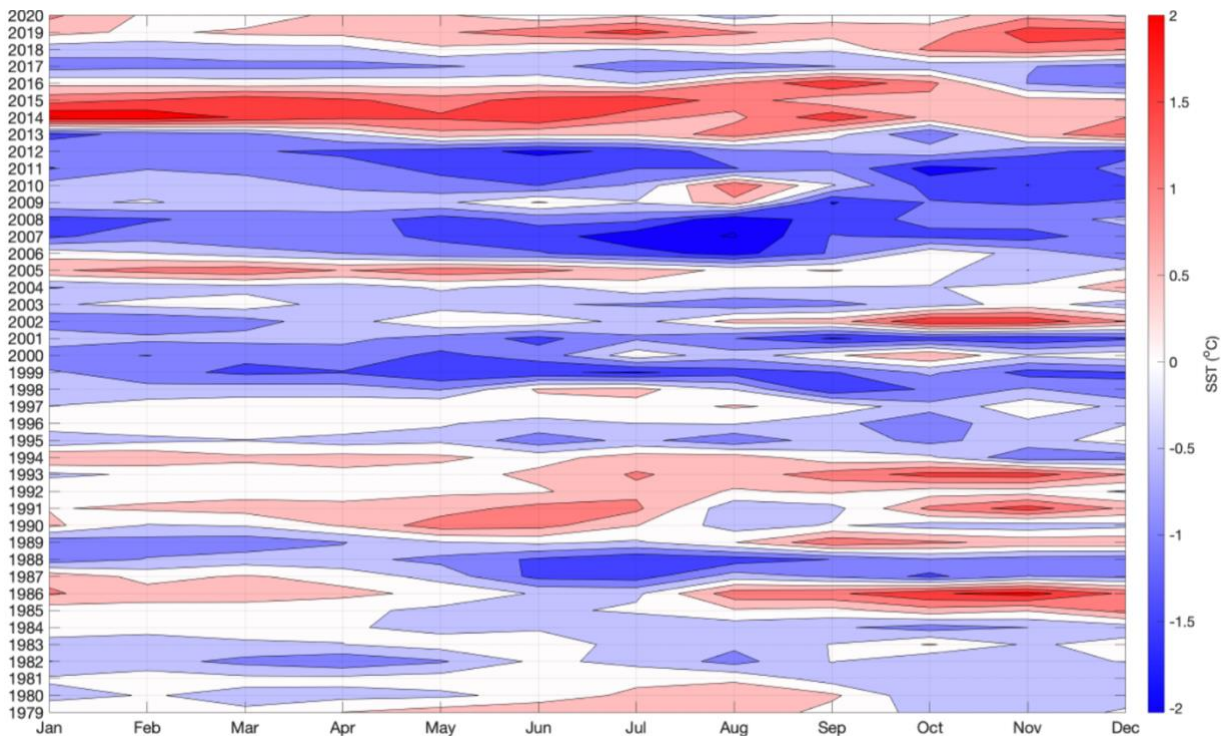


Figure 2. Timeseries of detrended monthly sea surface temperatures (°C) in the NEP focus region (1979-2020).

We detect warm events similar to the 2013-2015 Blob and the 2019 Blob 2.0 in the NEP as early as 1979 when the multidecadal warming trend is removed (Figure 2), suggesting that MHWs have been around longer than the most recent decade and are becoming more noticeable

with increasing frequencies and persistence with climate change. Besides the positive SSTAs that represent warm anomalies, there are multiple cool events of similar magnitude that appear to show interannual variation with the positive anomalies. The most recent events persisted for multiple years and were strong in the spring, summer, and winter. Earlier warm events in the 1980s and 1990s also show strong summertime anomalies (Figure 2). The warm and cool anomalies have gotten greater in magnitude in the most recent 20 years.

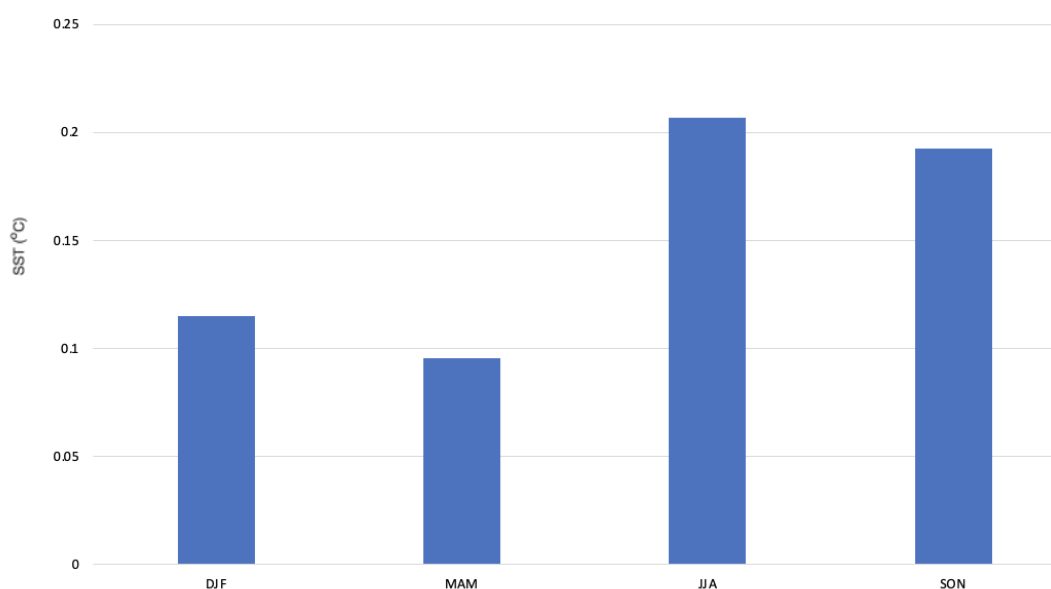


Figure 3. Seasonally averaged detrended sea surface temperature anomalies (°C) in the NEP focus region (1979-2020).

The NEP focus region, on average since 1979, had positive anomalies in all seasons of the year (Figure 3). On average, the SSTAs were strongest in the JJA and SON while smallest in the DJF and MAM. The anomalies in JJA have been almost twice as strong as the winter and spring anomalies. The focus of the rest of the study remains on air-sea interactions in the summer, JJA, along with interactions during the prior spring, MAM, that may have contributed to the positive summer SSTAs.

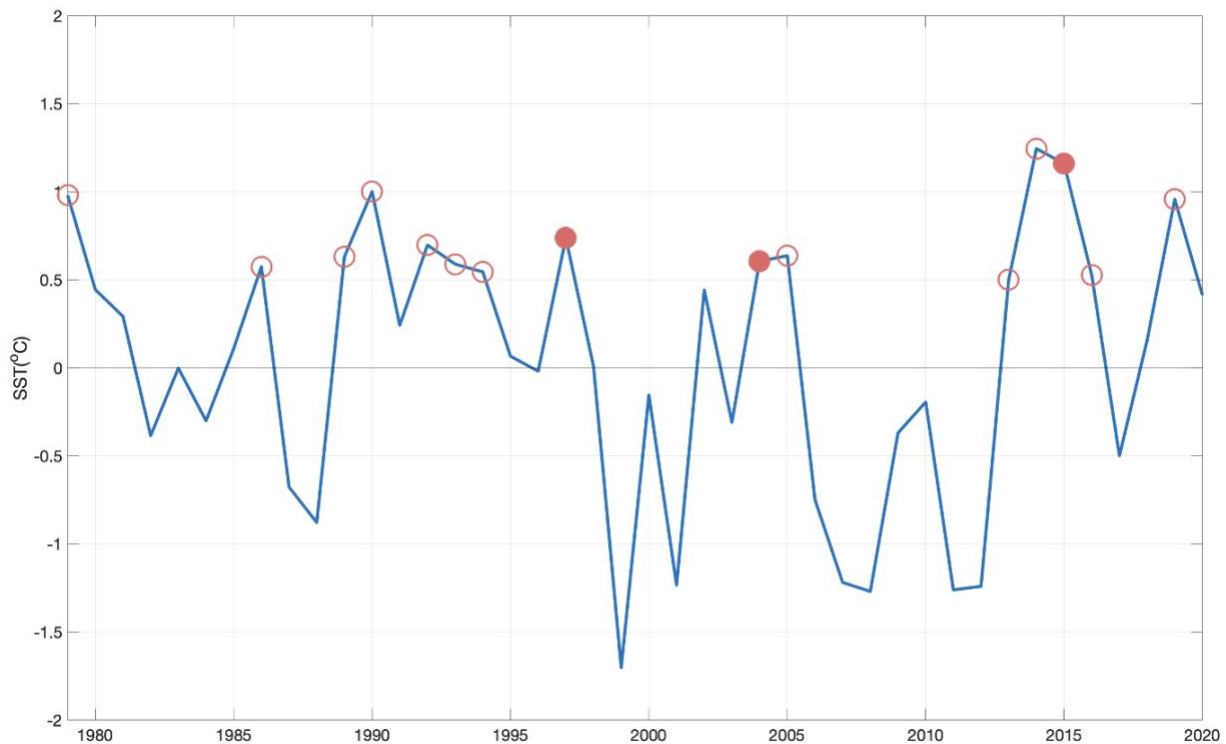


Figure 4. Timeseries of detrended Jun-Aug sea surface temperatures (°C) in the NEP focus region (1979-2020) with warm events identified by open red circles. The three filled red circles represent three warm events that occurred during an El Niño event that occurred in Jun-Aug.

As mentioned in the methods, the JJA warm events are identified from the 15 greatest SSTAs from the detrended SSTAs in the focus region from 1979 to 2020. As seen in Figure 2, there is evidence of interannual variation between positive and negative SSTAs in the focus region once the multidecadal trend is removed (Figure 4). The multidecadal trend removed from the timeseries was 0.067°C per decade (1979-2020) signifying a general warming trend in the NEP. However, when the trend is removed, the Blob and the Blob 2.0 had comparable magnitudes to much earlier warm events (Figure 4). Going forward in this analysis, it is

important to mention that only three of the 15 warm events occurred simultaneously with a JJA El Niño (filled circles in Figure 4).

Table 1. Warm events with associated sea surface temperature values (°C; in descending order) and ONI index recorded during Jun-Aug.

Warm Event Years	SST (°C) Detrended Value	JJA ONI Index
2014	1.24	0
2015	1.16	1.5
1990	1.00	0.3
1979	0.98	0
2019	0.96	0.3
1997	0.74	1.6
1992	0.70	0.4
2005	0.64	-0.1
1989	0.63	-0.3
2004	0.61	0.5
1993	0.59	0.3
1986	0.57	0.2
1994	0.55	0.4
2016	0.53	-0.4
2013	0.50	-0.4

Of the warm events identified from the detrended JJA SSTAs in the focus region, the anomalies for each event were all at least 0.5°C (Table 1). ‘The Blob’, which occurred during the summers of 2014 and 2015, was the strongest of the 15 warm events, and the ‘Blob 2.0’ ranked #5. Most of the warm events occurred during a neutral phase of ENSO with very few being in the El Niño phase (Figure 4 and Table 1).

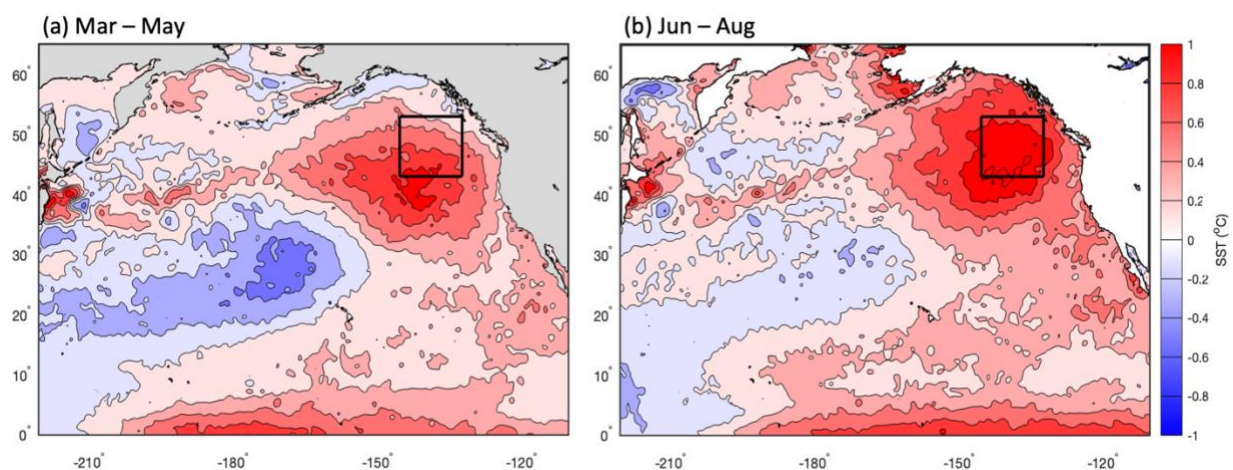


Figure 5. Observed sea surface temperature composite anomalies (°C) in the NEP (a) in Mar-May, prior to Jun-Aug warm events and (b) during warm events in Jun-Aug.

The center of the warm events (and the region that contains the largest anomalies) is roughly in the black box (Figure 1), or ‘focus region’, for both spring and summer (Figure 5). The warm events are seen in summer with a negative anomaly in the central Pacific of similar magnitude (Figure 5a). Averaged over all the warm events, the maximum warm event SSTA is around 1°C. As summer approaches, the warm events reach much of the coast of Alaska, Canada, and the western United States and the magnitudes of the positive anomalies strengthen (Figure 5b). The negative anomaly in summer is similar in location to the spring anomalies, yet weaker in magnitude (Figure 5b). In both seasons, the warm anomalies extend to the tropics along the eastern Pacific basin.

Surface Energy Budget Analysis

Figure 6 shows the terms of the surface energy budget equation presented on the right-hand side of Equation 2 before and during the summer warm events in the NEP. The surface energy budget analysis presents: (a) varying anomalies between MAM and JJA; and (b) that the main contributor to summer SSTAs in the NEP appears to come from a change in the atmosphere directly above the NEP.

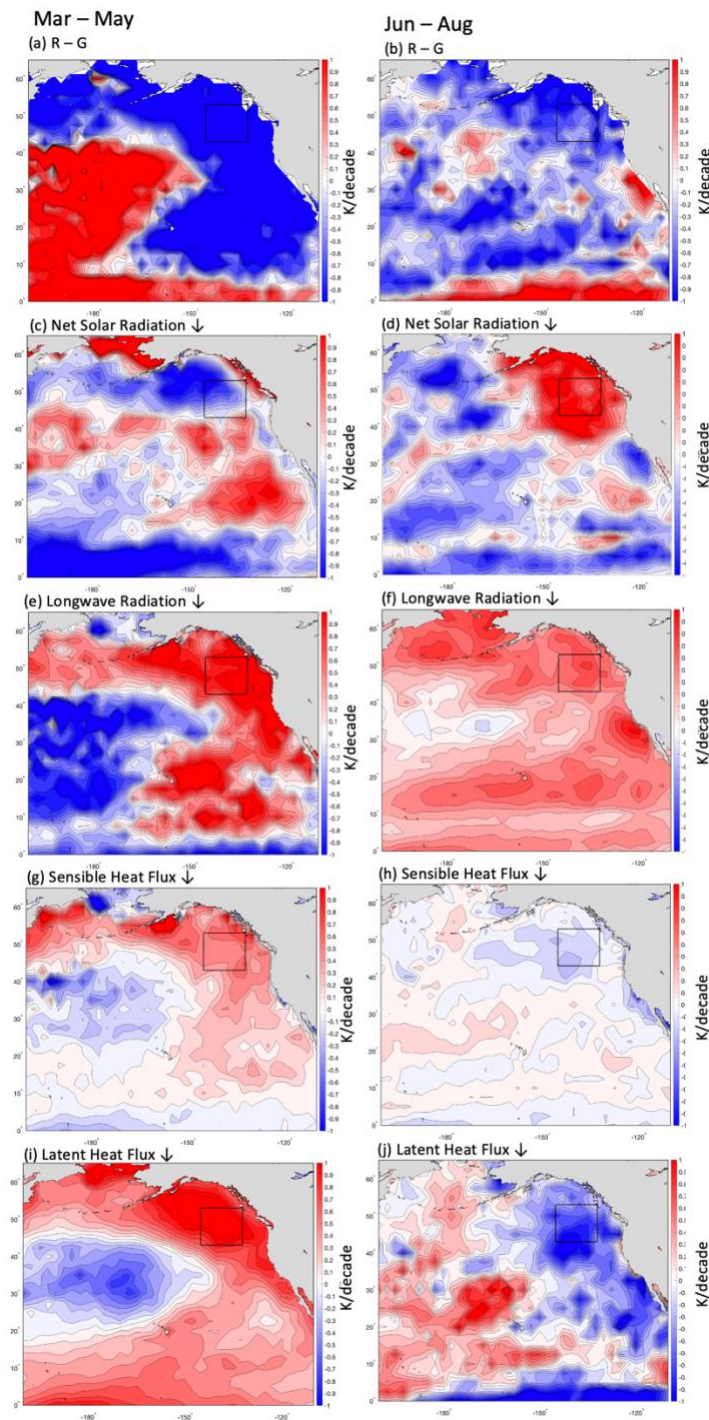


Figure 6. Surface energy budget component composite anomalous (a & b) R-G, (c & d) downward net solar radiation, (e & f) downward net longwave radiation, (g & h) downward sensible heat flux, and (i & j) downward surface latent heat flux contributions to the SSTAs for Mar-May (left column) and Jun-Aug (right column) in K per decade (Equation 2).

Because the previous section stressed the importance of focusing on the summer warm events, the summer surface budget analysis was performed along with the prior season. The spring surface budget analysis was performed to illustrate the difference between the seasons before and during the warm events. The spring R-G term, which includes influences from the ocean, has large negative changes in temperature per decade (over -1 K/decade) in the region of interest (Figure 6a) suggests that the ocean may play a factor in the energy exchange prior to the summertime SSTAs. The spring R-G term is of similar magnitude and opposite sign of the spring downward latent heat flux (Figure 6i), suggesting that the increased downward latent heat energy coming into the ocean is balanced by physical ocean variations (e.g., ocean divergence and temperature advection). The negative downward net solar radiation anomalies and the positive longwave radiation anomalies in the spring (Figure 6c, g) suggest that the focus region experienced less sun exposure than typical in the spring. The contribution of positive downward sensible heat flux anomalies is of small magnitude (about 0.3 K/decade) and may not play a significant role in the energy exchange that leads to the summer SSTAs.

In the summertime, the negative R-G anomaly contributes less to the change in temperature (about -0.3 K/decade) when compared to the springtime (Figure 6b). The summer anomaly signs are opposite for the net solar radiation and latent heat flux to those for the spring (Figure 6d, j) indicating that the circulation and cloud coverage changed between the two seasons. Two terms of similar magnitude that appear to balance each other in the focus region as well as much of the Pacific in the summertime are the net downward solar radiation and the latent heat flux (Figure 6d, f). The increased downward net solar radiation may be a result of a

change in circulation anomalies above the Pacific Ocean. As in spring, the longwave radiation and sensible heat fluxes are not major in terms of the energy budget for the warm events (Figure 6f, h). The next section goes into more detail about the change in atmospheric circulation observed above the NEP that led to the summer surface energy budget.

Summertime External Forcing

In this section, we focus on the observed atmospheric circulation and topical latent heat anomalies acting as external forcing. This section includes results from model simulations that use parts of the global latent heat anomalies observed during warm events to pinpoint the source of external forcing.

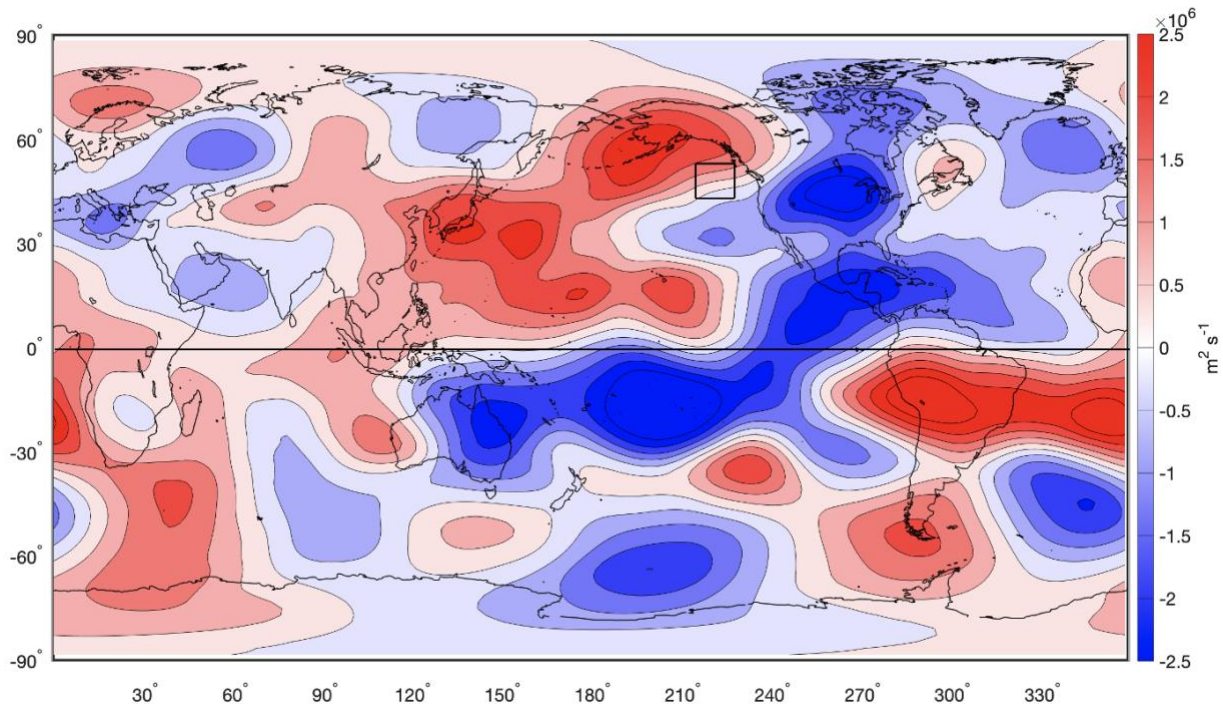


Figure 7. Observed 300 mb eddy streamfunction composite anomalies ($\text{m}^2 \text{s}^{-1}$) during warm events in Jun-Aug.

The composite JJA upper-tropospheric circulation anomalies for warm events are shown in Figure 7. Note the positive-negative dipole in 300 mb streamfunction anomalies over the focus region and the NEP in general. This dipole suggests anomalous geostrophic westward winds (going against the climatological eastward winds). We can also see two anomalous dipoles straddling the equator in the Pacific, with the larger dipole centered around 200°E (Figure 7). This dipole is consistent with anomalous heating on the equator (Gill 1980). These anomalies

suggest evidence for Rossby wave propagation from the central tropical Pacific (CTP) to the atmosphere anomalies that induce atmospheric anomalies necessary for the development of the warm events in the NEP. There is also a zonal and gently arching wave train that passes over Asia, North Pacific, North America, and North Atlantic that is also consistent with heating coming from the Maritime Continent/Southeast Asian region (as found in Sardeshmukh and Hoskins, 1988).

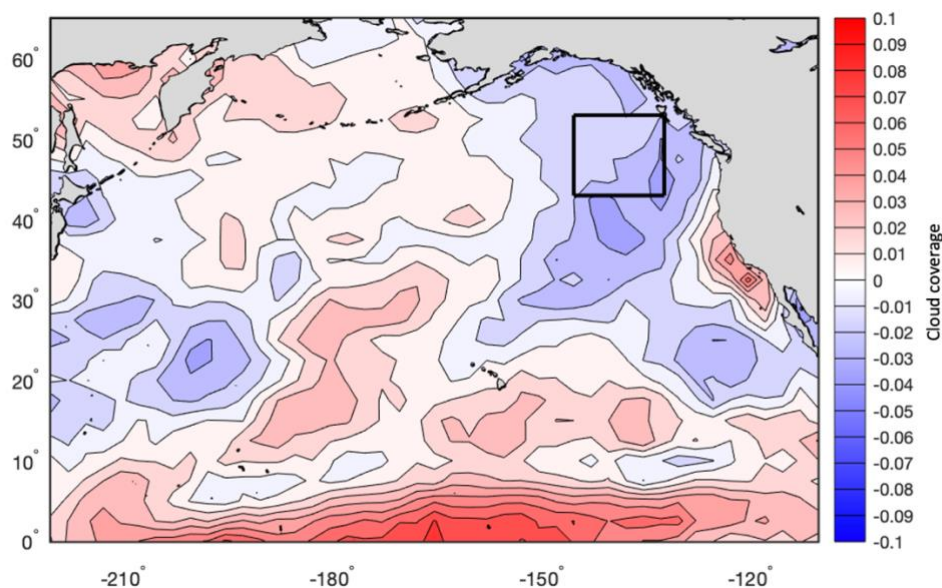


Figure 8. Composite anomalies for cloud coverage (negative = less clouds & positive = more clouds) in Jun-Aug for warm events.

The anomalously higher heights within and north of the region of interest (Figure 7) correspond to the anomalous decrease in cloud cover (Figure 8) that would increase the solar radiation needed to drive the summertime SSTAs that are suggested in Figure 6g. The decreased cloud coverage and increased solar radiation are consistent with findings from Amaya et al. (2021) that suggest that the main drivers for SSTAs events like the Blob 2.0 are driven by trapping solar heat in the upper ocean.

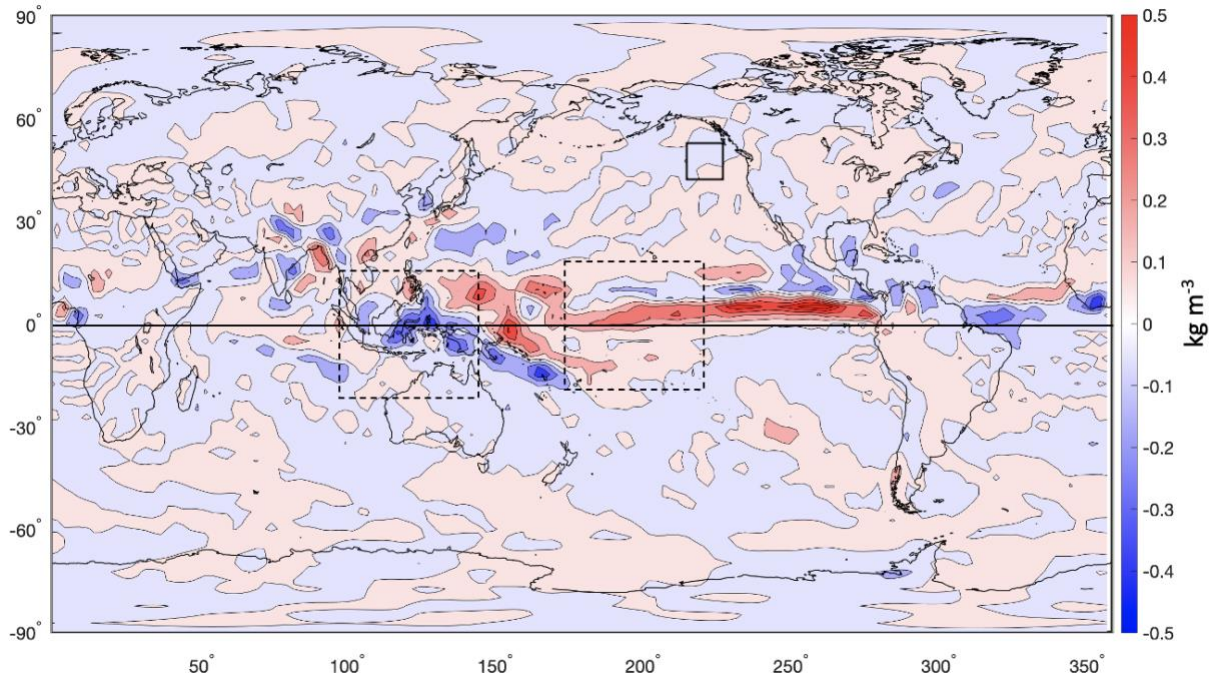


Figure 9. Observed latent heat anomalies (kg m^{-3}) averaged throughout the atmospheric column during warm events in Jun-Aug. Dashed boxes represent regions of interest for anomalous tropical heat forcing.

The observational analysis associated with Figures 6 and 7 raises the possibility that there may be latent heat anomalies in the equatorial region that force the observed atmospheric circulation. Directly under the equatorial dipole anomalies observed in Figure 7, there are strong anomalous heating fields present (Figure 9). The strongest positive anomalies ($>0.3 \text{ kg m}^{-3}$) tend to be present in the western, eastern, and central tropical Pacific. Over the Maritime Continent (MC), there are negative anomalies of similar magnitude (around -0.3 kg m^{-3}). The heating pattern over Southeastern Asia is more complicated with multiple positive and negative anomalies of lesser magnitude compared to the previously mentioned anomalies. The boxes with dashed borders in Figure 9 are discussed in more detail later.

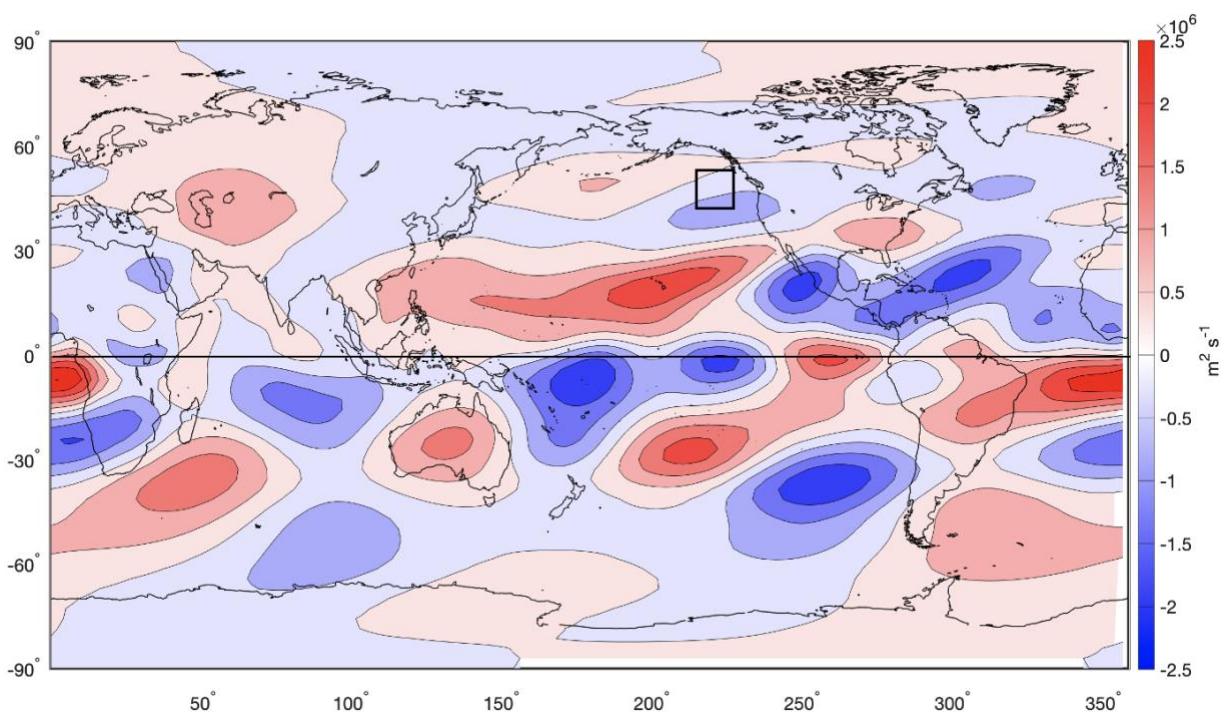


Figure 10. Model output of Jun-Aug 300 mb eddy streamfunction anomalies ($\text{m}^2 \text{s}^{-1}$) forced by the global heating field shown in Figure 9.

Now that there are known latent heat anomalies in the tropics, it is time to investigate if the heating anomalies can excite the observed circulation pattern for warm events. This is done by first forcing the model with the entire globe's latent heat anomalies (shown in Figure 9). When the model, with JJA background flow, is forced with the global observed JJA latent heating composite anomalies for warm events (Figure 9), the model output (Figure 10) slightly resembles the atmospheric patterns observed in certain regions (Figure 7). The model output captures the equatorial dipoles over the dateline and in the eastern equatorial Pacific. Similarly, the observed dipole directly over the focus region (Figure 7), is captured with a faint positive 300 mb streamfunction anomaly northwest of the focus region and a negative anomaly southeast of the box (Figure 10). Focusing on different heating regions and different atmospheric regions may

show the initiation/progression of Rossby wave trains that act to create warm events in the NEP.

With a pattern correlation coefficient of only 0.15, the model output (Figure 10) is not nearly an exact match to the observed circulation pattern (Figure 7), suggesting that a deeper analysis is required.

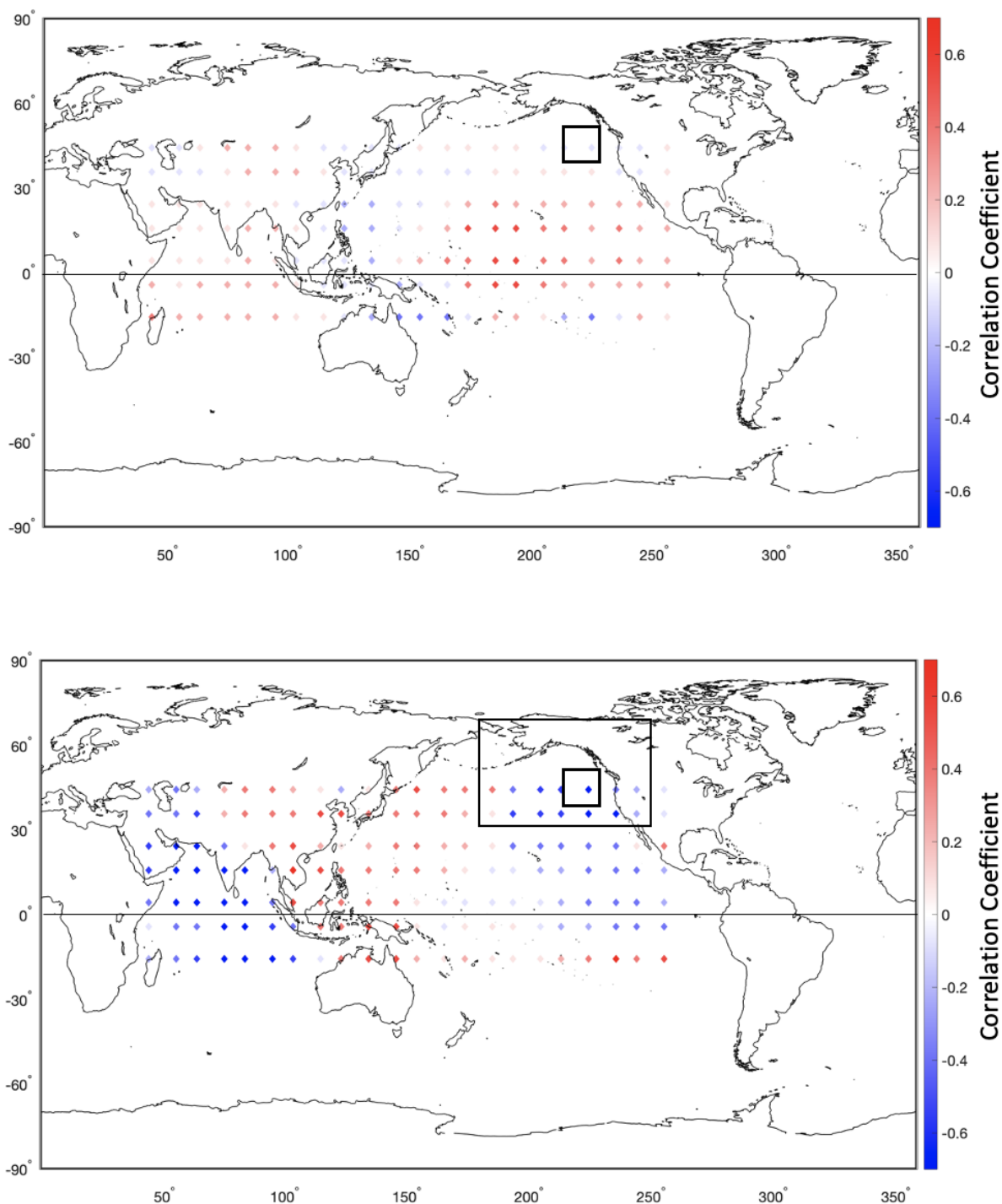


Figure 11. Pattern correlation map of 30°x30° patches (ranging from -30°-60°N to 30°-270°E) of model outputs of given patch observed Jun-Aug latent heating anomalies (represented by contoured diamond in the center of a given patch) correlated to observed of Jun-Aug 300 mb eddy streamfunction anomalies ($\text{m}^2 \text{s}^{-1}$) (a) globally and (b) within a 30°-70°N and 170°-250°E region (black).

Focusing on different heating regions and different atmospheric regions may show the initiation/progression of Rossby wave trains that act to create warm events in the northeastern Pacific. To investigate which areas of latent heating are most important in generating the observed circulation anomaly, a patch experiment similar to that described in Kim and Lee (2021) is performed. This experiment forces the model, with the JJA climatology as the background state, with observed latent heating composite anomalies in $30^{\circ}\times 30^{\circ}$ patches. These patches overlap each other by 10-degree increments in both the latitudinal and the longitudinal directions. Collectively, the patches used in this experiment cover -30°N - 60°N and 30°E - 270°E . The circulation model response of each patch model output is then correlated to the observed JJA 300 mb streamfunction anomalies. For example, a patch of observed latent heating during warm events (from 0°N - 30°N and 30°E - 60°E) forces the model and produces streamfunction anomaly outputs, which are then pattern correlated to the observed streamfunction anomalies of warm events. The correlation coefficient is represented by the diamond in the center of the patch's location and is presented along with the other patch correlations in Figure 11. Two different domains are pattern correlated: one is the full globe (Figure 11a), and the other is a smaller region (30°N - 70°N and 170°E - 250°E) focused more over the NEP (Figure 11b).

Table 2. Locations of the top positively correlated patches for JJA 300 mb streamfunction anomalies.

Global Correlation			Regional Correlation [30°-70°N and 170°-250°E]		
<i>Latitude</i>	<i>Longitude</i>	<i>R value</i>	<i>Latitude</i>	<i>Longitude</i>	<i>R value</i>
-20 °	170 °	0.45	-30 °	120 °	0.49
-10 °	170 °	0.47	-20 °	130 °	0.49
-10 °	180 °	0.46	-10 °	90 °	0.54
0 °	170 °	0.47	0 °	90 °	0.76
0 °	180 °	0.45	20 °	100 °	0.5

When the patches are correlated to the entire observed global 300 mb streamfunction anomaly field (Figure 11a), the strongest positive correlations, with correlation coefficients all greater than 0.44 (Table 2), occur in the CTP region. When the patches were correlated to just the observed 300 mb streamfunction anomaly field focused on the NEP at 30°N-70°N and 170°E-250°E (Figure 11b), the strongest positive correlations, with correlation coefficients all greater than 0.48 (Table 2), mostly occurred in the MC region (with the exception of one patch existing slightly north of the MC).

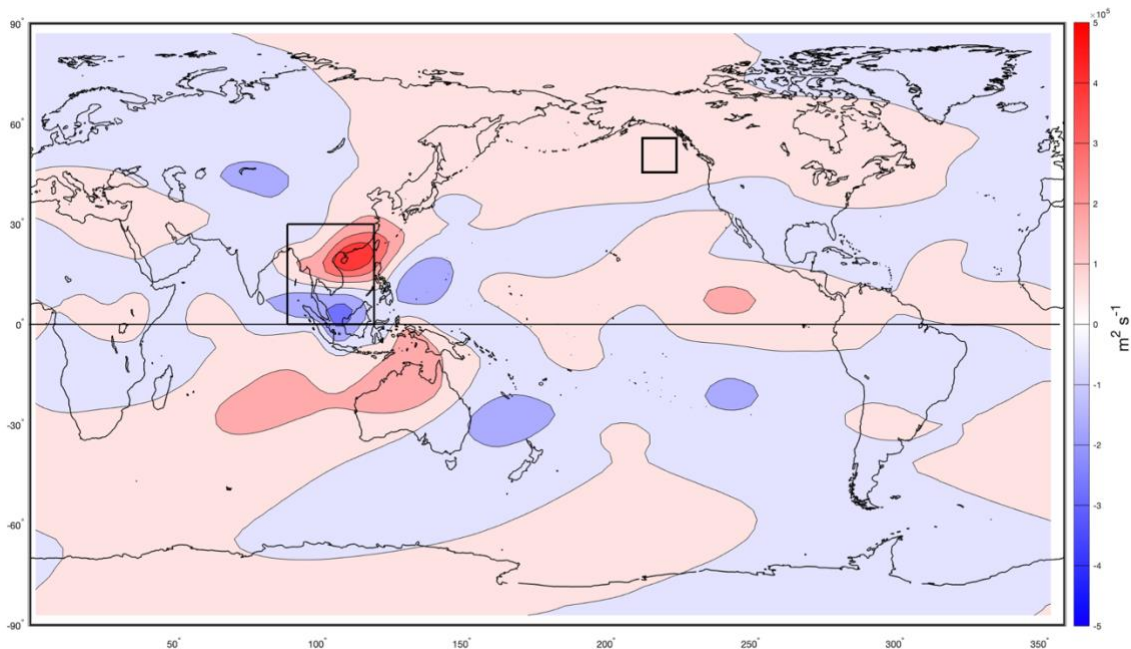


Figure 12. JJA model output 300 mb eddy streamfunction anomalies (m^2s^{-1}) from the patch, $0^\circ\text{-}30^\circ\text{N}$ and $90^\circ\text{-}120^\circ\text{E}$, that had the highest correlation coefficient (0.76 as shown in Table 2) when correlated to the atmospheric circulation within $30^\circ\text{-}70^\circ\text{N}$ and $170^\circ\text{-}250^\circ\text{E}$.

The model output of the patch with the highest correlation ($0^\circ\text{-}30^\circ\text{N}$ and $90^\circ\text{-}120^\circ\text{E}$) to the regional atmospheric circulation anomalies observed in Figure 7 exhibits a slight dipole over the focus region as well as the tropical heating anomalies observed during warm events (Figure 12). Note that the scale used for the model output streamfunction anomalies is different from the observed due to weaker anomalies from the model compared to the observed. The forcing from this patch also shows the initiation of a wave train extending from the MC over the Pacific Ocean in both the Northern and Southern Hemispheres.

The results of the two general regions of MC and CTP having high correlations suggest that multiple regions may both play a role in generating atmospheric anomalies in the tropics that influence the extratropics and the initiation of warm events in the NEP.

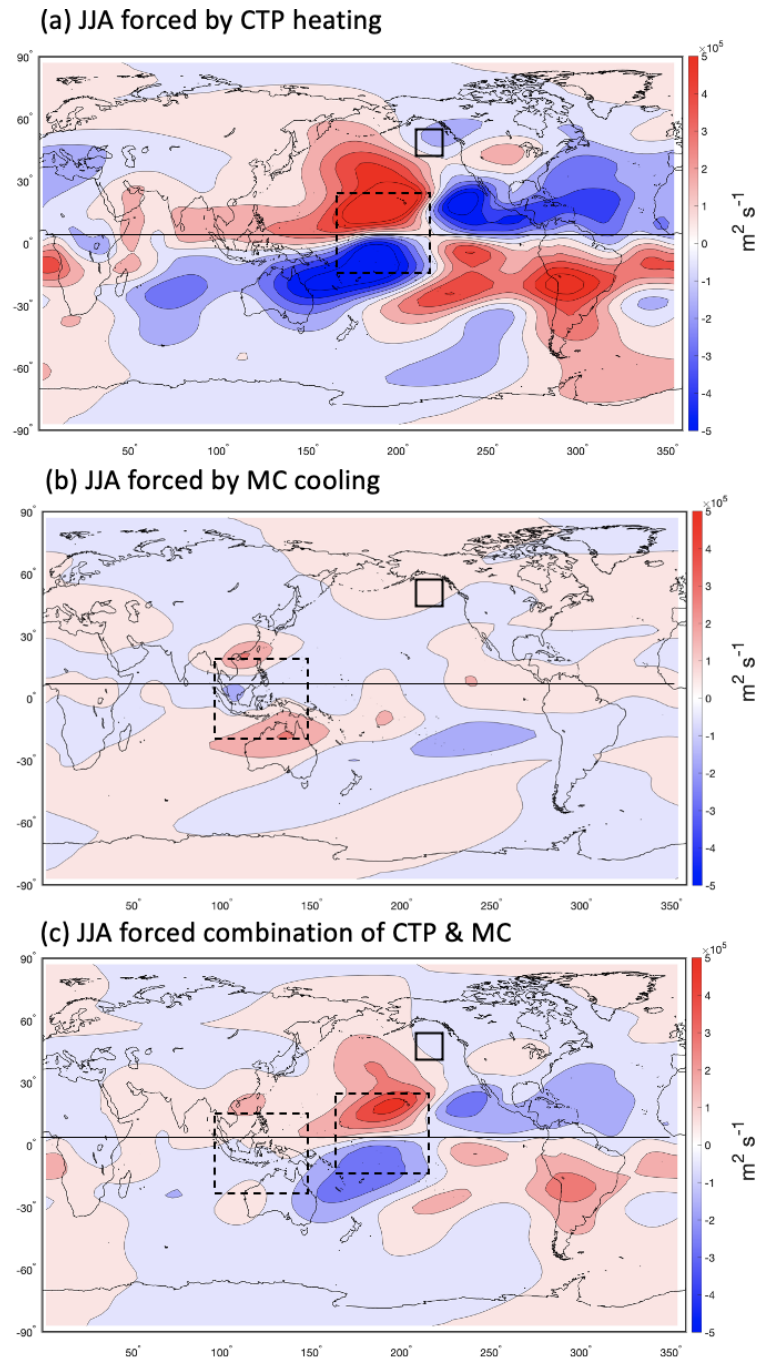


Figure 13. JJA model output 300 mb eddy streamfunction anomalies ($\text{m}^2 \text{s}^{-1}$) from (a) the central tropical Pacific, (b) the Maritime Continent, and (c) both the central tropical Pacific and Maritime Continent combined. Dashed boxes representing regions of interest for heat forcing. *

*Note that the dashed box in Figure 13b does not explicitly capture the patch with a southwest corner of 20°N and 100°E for simplicity, although the plot in Figure 13b does include its output.

The CTP region is composed of the 5 boxes shown in Table 2 (all of which had a correlation coefficient greater than 0.44 to the global atmospheric anomalies in the NEP as shown in Figure 13a) and generally consists of positive heating anomalies (Figure 9). The anomalous positive heating field in the CTP generates two clear streamfunction dipoles centered around the equator at about 200°E and 240°E observed in Figure 7 along with positive anomalies over the general west Pacific region.

The MC region is composed of the 5 boxes shown in Table 2 (all of which had a correlation coefficient greater than 0.48 to the atmospheric anomalies in the NEP as shown in Figure 13b) and generally consists of negative heating anomalies (Figure 9). Although relatively weak, the MC cooling region forces positive streamfunction anomalies northwest of the focus region just as seen in Figure 7. There are also clear arcing wave trains emanating from near the MC across the Pacific in both hemispheres (Figure 13b).

Combining the heating of CTP and MC, the model produces a circulation pattern (Figure 13c) that is faintly similar to the observed streamfunction anomalies shown in Figure 7 that suggests interference between wave trains initiated by the MC and CTP heating anomalies. In particular, there are positive streamfunction anomalies in the western Pacific that extend to the NEP just northwest of the focus region and there is a tropical heating-induced dipole around the equator. The resulting output of the combination of the two regions has a correlation coefficient of 0.46 to the observed JJA 300 mb streamfunction anomalies for warm events (Figure 13c).

Discussion

The study presented here has shown how interesting the NEP warm events have been since 1979. Warm events (and MHWs) are regular and tend to shift back and forth with anomalies of opposite signs (Figures 2 and 4). However, multi-decadal trends associated with climate change can make the warm (cool) events more (less) obvious, especially the more recent events (Figure 4). Because there is such variation between positive and negative anomalies in the NEP, it often can make predictability difficult in this region. Events similar to the Blob and Blob 2.0 have been occurring since 1979 (Figures 2 and 4). Considering that these NEP SSTAs have become more intense and have lasted longer in more recent years, the results in this study align well with Laufkötter et al. (2020) and Holbrook et al. (2019) in suggesting that these anomalies are becoming more intense due to climate change. This study chose to look solely at the summer season because the summer NEP SSTAs had the largest anomalies compared to the other seasons within a calendar year (Figure 3). Most NEP warm events occur without corresponding ENSO events (Figure 4). This suggests that other factors besides ENSO are the main drivers of these warm events.

The NEP warm events appear to be heavily affected by the air-sea energy exchanges (Figure 6) in the NEP compared to the small air-sea flux anomalies that Fewings and Brown (2019) found associated with 'The Blob' along the California Coast. The energy budget revealed that the downward net solar radiation was the main driver in the summer warm events. Amaya et al. (2021) suggest that the main driver of the Blob 2.0 was an anomalously shallow MLD, which shoaled as a result of increased solar heating, similar to this study. Further investigations are

needed to test the impact of MLD anomalies with the NEP warm events. The anomalous increased solar radiation is consistent with an upper atmospheric circulation change (Figures 7 and 8). The region above the focus region was found to have anomalously higher heights (Figure 7) and thus reduced cloud coverage (Figure 8). The increased warming in the uppermost ocean layer appears to be the main driver of summer positive SSTAs in the NEP.

The results of this study also illustrate that the observed atmospheric anomalies exhibit a teleconnection from the tropics through Rossby wave propagation to the NEP. The connection found here supports the tropical heating pattern suggested in Gill (1980) which has been shown by Hoskins and Karoly (1981) to reveal a teleconnection from the tropics to higher latitudes. During warm events, the CTP had positive latent heating anomalies right under the observed tropical atmospheric dipole anomaly, while the MC generally had negative latent heating anomalies. The model simulations revealed that the summertime CTP enhanced heating and MC suppressed heating anomalies are important in creating the observed dipole and the high heights in the NEP that lead to increased solar radiation heating (Figures 11 and 13).

Although the findings presented here are focused on NEP summer events, we recognize that this study is merely a one-season study that is not inclusive of the entire calendar year and the associated seasonal processes. Expanding the work here to the prior winter and spring may prove useful in understanding more of the connection (or no connection) to ENSO, considering ENSO is typically strongest in the winter season.

We also recognized that the model results here are forced by a fixed state, not a time-evolving forcing. A time-evolving forcing could provide clearer results when forcing the model for the MC heating anomalies as used in Kim and Lee (2021). The GFDL model is often also more accurate when the temporal resolution of the forcing and background state is reduced. Here an entire season is averaged and used, but if daily data along with time-evolving forcing were integrated into this study, there could be greater evidence of the MC tropical forcing and the extratropics. Another caveat of the model is that it uses fourth-order horizontal diffusion rather than eddy vorticity fluxes which could influence the tropical to extratropical connection.

Conclusion

Large masses of warmer-than-normal surface waters have been making an appearance in the NEP for over half a century. In the most recent decade, these warm water masses have increased in size, magnitude, and duration, earning the title of a ‘marine heatwave.’ In the summer season, these regions appear to be most influenced by atmospheric anomalies directly above the ocean that reduce wind speeds and increase solar heating. These atmospheric anomalies are part of constructively interfering wave trains emanating from the maritime continent and the central tropical Pacific due to suppressed and enhanced heating anomalies. The teleconnections that are part of the warm events extend east of the northeastern Pacific and thus may be important in creating anomalies over North America (including anomalies such as the ridging anomalies that produced the terrestrial heat wave in the Pacific Northwest in June 2021). There is great importance in understanding the physical structure and evolution of these sea surface temperature events in order to increase the ability to predict them. Communities along the Pacific Northwest Coast (i.e., fisheries, tribal communities, environmental protection agencies, etc.) rely heavily on the information provided about ocean conditions. With marine heatwaves occurring right off the coast and the associated alterations of surrounding ecosystems, there is great urgency to continue to understand these events as the climate continues to rapidly change.

BIBLIOGRAPHY

- Amaya, D. J., A. J. Miller, S.-P. Xie, and Y. Kosaka, 2020: Physical drivers of the summer 2019 North Pacific marine heatwave. *Nat Commun*, **11**, <https://doi.org/10.1038/s41467-020-15820-w>.
- Amaya, D. J., M. A. Alexander, A. Capotondi, C. Deser, K. B. Karnauskas, A. J. Miller, and N. J. Mantua, 2021: Are Long-Term Changes in Mixed Layer Depth Influencing North Pacific Marine Heatwaves? *Bulletin of the American Meteorological Society*, **102**, S59–S66, <https://doi.org/10.1175/bams-d-20-0144.1>.
- Baggett, C., S. Lee, and S. Feldstein, 2016: An Investigation of the Presence of Atmospheric Rivers over the North Pacific during Planetary-Scale Wave Life Cycles and Their Role in Arctic Warming. *Journal of the Atmospheric Sciences*, **73**, 4329–4347, <https://doi.org/10.1175/jas-d-16-0033.1>.
- Benthuyssen, J. A., H. Tonin, R. Brinkman, M. Herzfeld, and C. Steinberg, 2016: Intrusive upwelling in the Central Great Barrier Reef. *J. Geophys. Res. Oceans*, **121**, 8395–8416, <https://doi.org/10.1002/2016jc012294>.
- Bond, N. A., M. F. Cronin, H. Freeland, and N. Mantua, 2015: Causes and impacts of the 2014 warm anomaly in the NE Pacific. *Geophys. Res. Lett.*, **42**, 3414–3420, <https://doi.org/10.1002/2015gl063306>.
- Cheung, W. W. L., and T. L. Frölicher, 2020: Marine heatwaves exacerbate climate change impacts for fisheries in the northeast Pacific. *Sci Rep*, **10**, <https://doi.org/10.1038/s41598-020-63650-z>.
- Clark, J. P., V. Shenoy, S. B. Feldstein, S. Lee, and M. Goss, 2021: The Role of Horizontal Temperature Advection in Arctic Amplification. *Journal of Climate*, **34**, 2957–2976, <https://doi.org/10.1175/jcli-d-19-0937.1>.
- Di Lorenzo, E., and N. Mantua, 2016: Multi-year persistence of the 2014/15 North Pacific marine heatwave. *Nature Clim Change*, **6**, 1042–1047, <https://doi.org/10.1038/nclimate3082>.
- Fewings, M. R., and K. S. Brown, 2019: Regional Structure in the Marine Heat Wave of Summer 2015 Off the Western United States. *Front. Mar. Sci.*, **6**, <https://doi.org/10.3389/fmars.2019.00564>.
- Frölicher, T. L., E. M. Fischer, and N. Gruber, 2018: Marine heatwaves under global warming. *Nature*, **560**, 360–364, <https://doi.org/10.1038/s41586-018-0383-9>.
- Gill, A. E., 1980: Some simple solutions for heat-induced tropical circulation. *Q.J Royal Met. Soc.*, **106**, 447–462, <https://doi.org/10.1002/qj.49710644905>.

- Held, I. M., and M. J. Suarez, 1994: A Proposal for the Intercomparison of the Dynamical Cores of Atmospheric General Circulation Models. *Bull. Amer. Meteor. Soc.*, **75**, 1825–1830, [https://doi.org/10.1175/1520-0477\(1994\)075<1825:apftio>2.0.co;2](https://doi.org/10.1175/1520-0477(1994)075<1825:apftio>2.0.co;2).
- Hersbach, H., and Coauthors, 2020: The ERA5 global reanalysis. *Q.J.R. Meteorol. Soc.*, **146**, 1999–2049, <https://doi.org/10.1002/qj.3803>.
- Hobday, A. J., and Coauthors, 2016: A hierarchical approach to defining marine heatwaves. *Progress in Oceanography*, **141**, 227–238, <https://doi.org/10.1016/j.pocean.2015.12.014>.
- Hobday, A., and Coauthors, 2018: Categorizing and Naming Marine Heatwaves. *Oceanog*, **31**, <https://doi.org/10.5670/oceanog.2018.205>.
- Holbrook, N. J., and Coauthors, 2019: A global assessment of marine heatwaves and their drivers. *Nat Commun*, **10**, <https://doi.org/10.1038/s41467-019-10206-z>.
- Hoskins, B. J., and D. J. Karoly, 1981: The Steady Linear Response of a Spherical Atmosphere to Thermal and Orographic Forcing. *J. Atmos. Sci.*, **38**, 1179–1196, [https://doi.org/10.1175/1520-0469\(1981\)038<1179:tslroa>2.0.co;2](https://doi.org/10.1175/1520-0469(1981)038<1179:tslroa>2.0.co;2).
- Joh, Y., and E. Di Lorenzo, 2017: Increasing Coupling Between NPGO and PDO Leads to Prolonged Marine Heatwaves in the Northeast Pacific. *Geophys. Res. Lett.*, **44**, 11,663–11,671, <https://doi.org/10.1002/2017gl075930>.
- Kim, D. W., and S. Lee, 2021: Relationship between Boreal Summer Circulation Trend and Destructive Stationary-Transient Wave Interference in the Western Hemisphere. *Journal of Climate*, 1–38, <https://doi.org/10.1175/jcli-d-20-0530.1>.
- Kim, D. W., and S. Lee, 2022: The Role of Latent Heating Anomalies in Exciting the Summertime Eurasian Circulation Trend Pattern and High Surface Temperature. *Journal of Climate*, **35**, 801–814, <https://doi.org/10.1175/jcli-d-21-0392.1>.
- Kobayashi, S., and Coauthors, 2015: The JRA-55 Reanalysis: General Specifications and Basic Characteristics. *Journal of the Meteorological Society of Japan*, **93**, 5–48, <https://doi.org/10.2151/jmsj.2015-001>.
- Laufkötter, C., J. Zscheischler, and T. L. Frölicher, 2020: High-impact marine heatwaves attributable to human-induced global warming. *Science*, **369**, 1621–1625, <https://doi.org/10.1126/science.aba0690>.
- Park, M., and S. Lee, 2021: Is the Stationary Wave Bias in CMIP5 Simulations Driven by Latent Heating Biases? *Geophys Res Lett*, **48**, <https://doi.org/10.1029/2020gl091678>.

- NOAA, 2019b: Cold and warm episodes by season, accessed 02 March 2022, https://origin.cpc.ncep.noaa.gov/products/analysis_monitoring/ensostuff/ONI_v5.php.
- Oliver, E. C. J., J. A. Benthuisen, N. L. Bindoff, A. J. Hobday, N. J. Holbrook, C. N. Mundy, and S. E. Perkins-Kirkpatrick, 2017: The unprecedented 2015/16 Tasman Sea marine heatwave. *Nat Commun*, **8**, <https://doi.org/10.1038/ncomms16101>.
- Oliver, E. C. J., J. A. Benthuisen, S. Darmaraki, M. G. Donat, A. J. Hobday, N. J. Holbrook, R. W. Schlegel, and A. Sen Gupta, 2021: Marine Heatwaves. *Annu. Rev. Mar. Sci.*, **13**, 313–342, <https://doi.org/10.1146/annurev-marine-032720-095144>.
- Pearce, A. F., and M. Feng, 2013: The rise and fall of the “marine heat wave” off Western Australia during the summer of 2010/2011. *Journal of Marine Systems*, **111–112**, 139–156, <https://doi.org/10.1016/j.jmarsys.2012.10.009>.
- Rodrigues, R. R., A. S. Taschetto, A. Sen Gupta, and G. R. Foltz, 2019: Common cause for severe droughts in South America and marine heatwaves in the South Atlantic. *Nat. Geosci.*, **12**, 620–626, <https://doi.org/10.1038/s41561-019-0393-8>.
- Sardeshmukh, P. D., and B. J. Hoskins, 1988: The Generation of Global Rotational Flow by Steady Idealized Tropical Divergence. *J. Atmos. Sci.*, **45**, 1228–1251, [https://doi.org/10.1175/1520-0469\(1988\)045<1228:tgogrf>2.0.co;2](https://doi.org/10.1175/1520-0469(1988)045<1228:tgogrf>2.0.co;2).
- Smale, D. A., and Coauthors, 2019: Marine heatwaves threaten global biodiversity and the provision of ecosystem services. *Nat. Clim. Chang.*, **9**, 306–312, <https://doi.org/10.1038/s41558-019-0412-1>.
- Sparnocchia, S., M. E. Schiano, P. Picco, R. Bozzano, and A. Cappelletti, 2006: The anomalous warming of summer 2003 in the surface layer of the Central Ligurian Sea (Western Mediterranean). *Ann. Geophys.*, **24**, 443–452, <https://doi.org/10.5194/angeo-24-443-2006>.
- Tanaka, K. R., and K. S. Van Houtan, 2022: The recent normalization of historical marine heat extremes. *PLOS Clim*, **1**, e0000007, <https://doi.org/10.1371/journal.pclm.0000007>.

ACADEMIC VITA

Catherine (Katie) KohlmanLinkedIn: www.linkedin.com/in/catherinekohlman

Education

Schreyer Honors College at the Pennsylvania State University	University Park, PA
B.S. in Meteorology and Atmospheric Science (Marine Science Minor)	May 2022

Research Interests

Physical Oceanography, Climate, Physical-Biological Interactions, Marine Heatwaves

Research Experience

PSU Department of Meteorology – University Park, PA	Fall 2020 – Present
<i>Undergraduate Honors Thesis (Advised by Sukyoung Lee & Tom Murphree)</i>	
Air-Sea Energy Analysis with Global Circulation Models of Northeastern Pacific Marine Heatwaves	

NOAA Pacific Marine Environmental Laboratory – Seattle, WA	Summer 2021
<i>Ernest F. Hollings Undergraduate Research Internship (Advised by Meghan Cronin & Robert Dziak)</i>	
Potential Impacts of the 2019 Marine Heatwave Observed at Station Papa	

Naval Postgraduate School – Monterey, CA	Summer 2020 – Present
<i>Undergraduate Student Research Intern (Advised by Tom Murphree)</i>	
The Role of Atmospheric Teleconnections in Generating Marine Heatwaves in the Eastern North Pacific	

PSU Department of Geoscience – University Park, PA	Spring 2019 – Fall 2019
<i>NASA PA Space Grant Consortium Research Internship (Advised by Roman DiBiase & Julia Carr)</i>	
Grain size mapping of rivers in the Taiwan Central Range using drone surveys	

Computer Skills: Python, MATLAB, NCL, RStudio, ArcGIS (Novice)

Publications*Manuscripts***Kohlman, K.**, Cronin, M., Dziak, R., Mellinger, D., Sutton, A., and Galbraith, M. Potential Impacts of the 2019 Marine Heatwave Observed at Station Papa. In Preparation.**Kohlman, K.**, Madden, S., and Murphree, T. The Role of Atmospheric Teleconnections in Generating Marine Heatwaves in the Eastern North Pacific. In Preparation.*Conference Proceedings***Kohlman, K.**, Madden, S., and Murphree, T. (2021) Marine Heatwaves in the Eastern North Pacific: Characteristics and Causes. Extended Summary, Climate Prediction S&T Digest, 45th NOAA Climate Diagnostics and Prediction Workshop, Virtual Online, DOC/NOAA, 121-127. DOI: 10.25923/tpfe-4n87

Presentations*Invited Talks*

NOAA OAR Headquarters' Oceans Portfolio Monthly Call – Virtual	Oct. 2021
Fisheries and Oceans Canada/Institute of Ocean Sciences (DFO/IOS) – Virtual	Sep. 2021

Oral Presentations

Ocean Sciences Meeting 2022 – Virtual	Feb. 2022
Hollings Scholar Final Presentation – Virtual	Aug. 2021
NOAA Pacific Marine Environmental Laboratory Student Symposium – Virtual	Aug. 2021
NOAA Climate Diagnostics and Prediction Workshop – Virtual	Oct. 2020

Posters

21st Annual Student Conference – Houston, TX	Jan. 2022
Celebration of Undergraduate Engagement – University Park, PA	Apr. 2021
• <i>Library Research Award</i>	
American Meteorological Society Student Conference – Virtual	Jan. 2021
American Geophysical Union Fall Meeting – Virtual	Dec. 2020

American Geophysical Union Fall Meeting – Virtual	Dec. 2020
Celebration of Undergraduate Engagement – University Park, PA	Apr. 2020
• <i>Best Sophomore Poster Award</i>	
NASA Space Grant WMF Research Symposium – University Park, PA	Dec. 2019

Awards and Honors

• NOAA Ernest F. Hollings Undergraduate Scholarship	2020 – Present
• Schreyer Honors College Scholarship	2020 – Present
• Chi Epsilon Pi Meteorological Honors Society	2020 – Present
• PSU EMS Strickler Honors Scholarship	2020 – Present
• College of Earth and Mineral Sciences Academy for Global Experience Laureate	2021
• American Meteorological Society Senior Named – Jay Fein Scholarship	2021
• PSU Nominee for the Astronaut Scholarship	2021
• PSU Student Engagement Network Grant	2021
• National Weather Association – Arthur C. Pike Scholarship	2020
• Acceptance into CSUMB REU Program (<i>cancelled due to COVID-19</i>)	2020
• The President’s Freshman Award	2019
• PSU EMS Tholan P. Stuart and Marilyn Scholarship	2019
• Dean’s List	2018 – Present
• PSU Provost Award	2018 – Present
• Phi Eta Sigma National Honor Society	2018 – Present
• PSU EMS Matthew J. Wilson Honors Scholarship	2018

Teaching Experience

Intensive English Communication Program – University Park, PA	Spring 2022
Morgan Academic Center – University Park, PA	Fall 2021
Chi Epsilon Pi Meteorological Honors Society – University Park, PA	Fall 2021
Learning Assistant for General Physics Mechanics – University Park, PA	Spring 2019

Professional Experience

State Climate Office Intern – University Park, PA	Spring 2020 & Fall 2021
California State University – Monterey Bay, CA	Summer 2020
Weather World Volunteer – University Park, PA	Fall 2018
Campus Weather Service – University Park, PA	Spring & Fall 2018
Pre-College Marine Science Camp – Eckerd College, FL	Summer 2017

Extra-Curricular and Leadership

College of Earth and Mineral Sciences Ambassador	2021
PSU Weather Data Science Club, Treasurer & Secretary 2020 – 2021	2020 – Present
College of EMS Academy for Global Experience, Practitioner & Laureate	2020 – Present
Women in Earth and Mineral Sciences, Secretary 2018, <i>Vice President</i> 2019	2018 – Present
Marine Science Society, Social Chair 2021 – 2022	2019 – Present
Nittany Divers Club	2019 – Present
Earth and Mineral Sciences Student Council/THON	2018 – Present
Earth and Mineral Science Special Living Option	Aug. 2018 – May 2020

Certifications

PADI Open Water Diver Certification – Wilmington, NC	2016
---	------

Community Service

The Carpenter’s Project of Ellwood City, PA, Crew Leader 2018 & 2019	Summers 2014 – 2020
PSU Alternative Spring Break Service Trip	March 2019
Yellow Ribbon Girls	Summers 2014 – 2019
Ellwood City Food Bank	Summers 2014 – 2019